Brownian dynamics simulation of tracer diffusion in a cross-linked network

Huai Zhou and Shing Bor Chen*
Department of Chemical & Biomolecular Engineering, National University of Singapore, Singapore 117576
(Received 13 October 2008; published 10 February 2009)

Brownian dynamics simulation is employed to study the self-diffusion of tracer particles in a cross-linked gel network based on a coarse-grained bead-spring lattice model. Several effects are investigated including the network porosity, flexibility, degree of cross linking, and electrostatic interaction. For uncharged systems, the tracer long-time diffusivity is found to decrease with deceasing porosity and flexibility, but with increasing degree of cross linking. For charged systems, the diffusion is further hindered by the electrostatic interaction, regardless of whether the tracer particle and the network are oppositely or similarly charged. However, there exists a difference in the hindrance mechanism between the two cases. For the former, a substantial decrease in the diffusivity can occur at high network porosities due to electrostatic entrapment.

DOI: 10.1103/PhysRevE.79.021801 PACS number(s): 82.35.−x, 66.10.C−

I. INTRODUCTION

Probe diffusion has been commonly used as a technique called microrheology to explore the dynamics and rheology of soft matters such as polymer solutions, colloidal gels, hydrogels, etc. [1]. The particle diffusion is strongly affected by its interaction with the constituents and the microstructure of the matter. In addition, diffusion is also of fundamental importance for the controlled release of drug molecules from a hydrogel that can change in volume in response to external stimuli such as a change in temperature or *p*H [2–4], and imposition of an electric field [5]. Therefore, understanding particle diffusion in a network is essential for a variety of practical applications. For the past two decades, computer simulation has proven adequate to investigate diffusion and dynamics in solutions of linear polyelectrolytes [6–9] or uncharged polymers [10–12].

Molecular dynamics [13,14] and Monte Carlo [15] simulations have both been used to study the diffusion of small molecules in a cross-linked polymer network, such as polyacrylamide gel. Although the detailed gel architecture and the local gel dynamics could be simulated, the system size was restricted to be quite small for the subsequent simulation of the penetrant diffusion [13,14]. Much longer simulations are needed for the investigation of the translational dynamics to calculate the statistically relevant translational diffusion coefficients, on a larger time scale that allows the probe molecules to undergo hopping between the local environments [14].

Miyata *et al.* used Brownian dynamics simulation to investigate the self-diffusion of a charged particle in a swollen countercharged hydrogel [16]. On the basis of a cubic lattice, the cross-linked polymers in the hydrogel were modeled by straight chains, each comprised of jointed tangent hard spheres. Such a cubic lattice model represents a rigid network, through which the tracer particle diffuses. They focused on the effect of attractive electrostatic interaction between the tracer and the network by varying the network charge density. The network porosity is kept high at 0.9994 such that the volume exclusion is comparatively unimportant. For the ionic strength ranging from $0.02M$ to $1M$, they found that the tracer diffusivity can be reduced substantially at high enough network charge density and low enough ionic strength. This significant hindrance to diffusion is attributed to the entrapment of tracer particles due to the electrostatic attraction.

The flexibility of a cross-linked network was considered by Teixeira and Licinio, who examined the anomalous diffusion of polymer segments based on a bead-spring model [17]. A three-dimensional (3D) gel is represented by a cubic lattice network, where a bead is placed on each cross-link point connecting to six adjacent points by Hookean springs. They calculated the average mean square displacement of beads subject to random and spring forces without volume exclusion effects. A similar simulation was also carried out for fractal networks [18]. Recently, dynamics light scattering was employed by Teixeria *et al.* to experimentally investigate the anomalous diffusion of polymer segments of poly (methyl methacrylate) gel and polyacrylamide gel [19]. They measured the intensity autocorrelation function caused by the submicron particles that were trapped during the gel synthesis. For such a system, the volume exclusion and network flexibility are both important. However, there exists no simulation work that takes the two effects into consideration. We are thus motivated to investigate the diffusion of tracer particles in a flexible cross-linked network, which is also allowed to carry charge.

In this paper, we conduct Brownian dynamics simulation to examine the diffusion of probe particles in a 3D flexible cross-linked network, which is modeled on the basis of a bead-spring cubic lattice similar to that used by Teixeira and Licinio [17]. The concentration of the probes is assumed to be very low so as to neglect their interaction. The degree of cross linking is adjustable via removal of some of the springs. The network and tracer particles can be either charged or uncharged. For the former case, the charge sign of the tracer can be the same as or opposite to that of the network. We incorporate the excluded volume effect, but neglect the hydrodynamic interactions between the beads and tracer particles.

*Corresponding author. checsb@nus.edu.sg

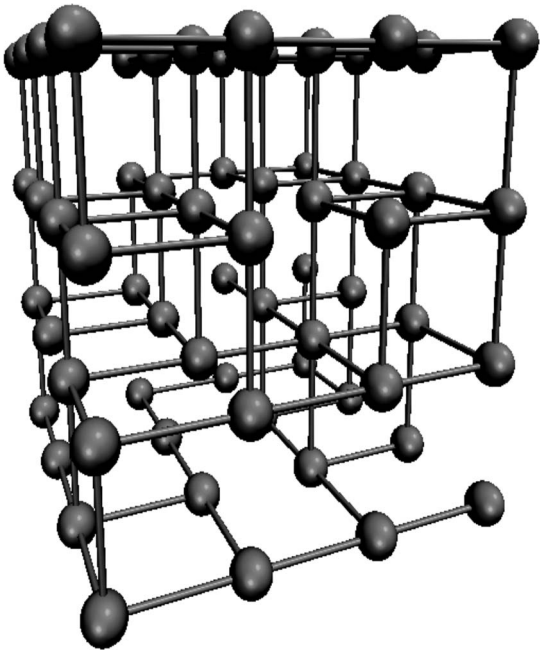

FIG. 1. Schematic of a bead-spring cross-linked network. Each stick connector represents a spring.

II. DESCRIPTION OF THE METHODS

The diffusion of a tracer particle in a polymeric gel is investigated by Brownian dynamics simulation. A simple cubic lattice comprised of cross-linked bead-spring chains is used to represent the gel network with the beads being located only at the cross-link points. We adopt a cubic simulation box of side length L, where N^3 network beads and a tracer particle are placed, and implement periodic boundary condition as usual. The degree of cross linking can be adjusted by removing some of the springs from the cubic lattice as illustrated in Fig. 1. In order to maintain the network connectivity, caution has been taken to ensure that no isolated segments result from such removal. The tracer and gel beads are of equal diameter σ, and are generically called particles hereafter. The solvent is treated as a continuum. The network porosity is defined as the volume fraction of free space: $\beta = 1 - \pi\sigma^3 N^3 / 6L^3$.

The dynamics of each of the particles is described by the Langevin equation

$$\zeta_i \frac{d\mathbf{r_i}}{dt} = -\nabla_{\mathbf{r_i}} \sum_{\substack{j=0 \\ j\neq i}}^{N^3} U_{ij} + \mathbf{R}_i, \quad (i = 0,1,\ldots,N^3), \tag{1}$$

where $\mathbf{r}_i$ and ζ_i are the position vector and friction coefficient of particle i ($i=0$ denoting the tracer), $\mathbf{R}_i$ is the random force due to the incessant collision of the solvent molecules with the particle, and U_{ij} is the pairwise interaction potential. The particle inertial effect has been neglected in Eq. (1) under the condition that the timescale is much larger than that for the relaxation of the particle momentum m_i/ζ_i, where m_i is the particle mass. In this study, we neglect the hydrodynamics interactions between the particles, and consider the steric, charge and flexibility effects with U_{ij} being expressed as

$$U_{ij} = U_{ij}^{\mathrm{ex}} + U_{ij}^{\mathrm{el}} + U_{ij}^{\mathrm{sp}} \tag{2}$$

where the superscripts "ex," "el," and "sp" denote the excluded volume effect, electrostatic interaction, and spring force (for adjacent network beads only), respectively.

TABLE I. Relation between l_0/σ and β.

l_0/σ	10	5	2.5	2	1.67	1.43	1.25
β	0.9995	0.996	0.966	0.934	0.886	0.818	0.728

For the network flexibility, we use the elastic potential energy of a harmonic spring for every two adjacent connected beads given by

$$U_{ij}^{\mathrm{sp}} = k(r_{ij} - l_0)^2 \tag{3}$$

where k is the spring constant, r_{ij} the center-to-center distance between the beads, and l_0 the equilibrium bond length, which is set equal to the corresponding distance in the rigid counterpart at the same porosity. Note that the length ratio l_0/σ is related to the network porosity by $l_0/\sigma = [6(1-\beta)/\pi]^{-1/3}$, and some selective values are listed in Table I. The steric effect is considered for nonconnecting particles, and is modeled by the truncated Lennard-Jones potential

$$U_{ij}^{\mathrm{ex}} = 4w\left[\left(\frac{\sigma}{r_{ij}}\right)^{12} - \left(\frac{\sigma}{r_{ij}}\right)^{6} + \frac{1}{4}\right] \tag{4}$$

with the energy depth $w = 1.2k_BT$ ($=4.9\times10^{-21}$ J at 25 °C) and the cutoff $r_C = 2^{1/6}\sigma$, where k_B is the Boltzmann constant, T is the absolute temperature, and σ can be regarded as the particle diameter (=5 nm). The parameter values are chosen to ensure a good solvent condition for the corresponding linear polymer. For the charge effect, we adopt the screened electrostatic interaction energy derived by Hogg *et al.* [20] and Wiese and Healy [21]:

$$U_{ij}^{\mathrm{el}} = \frac{\pi\varepsilon_0\varepsilon_r\sigma}{4}(\psi_i^2 + \psi_j^2)\left(\frac{2\psi_i\psi_j}{\psi_i^2 + \psi_j^2}\ln\frac{1+\exp(-H/\lambda)}{1-\exp(-H/\lambda)} - \ln[1-\exp(-2H/\lambda)]\right), \tag{5}$$

where ε_0 is the permittivity of a vacuum, ε_r the dielectric constant of water, λ the Debye screening length characterizing the double layer thickness, H the minimum separation distance between the surfaces of particles, and ψ_i the surface electrical potential when particle i is isolated. The relation between ψ_i and particle charge Q_i is

$$\psi_i = \frac{\lambda Q_i}{\pi\sigma^3\varepsilon_0\varepsilon_r}. \tag{6}$$

At high enough ionic strength, Eq. (5) is superior to the simple Debye-Huckel model, because the latter regards particles as charge points, thereby requiring a thick double layer. To take into account possible counterion condensation, one can use the effective charge on each particle.

The time evolution of the position of each particle is determined by numerically integrating Eq. (1). Hereafter, we

normalize all lengths by σ, energy by k_BT, particle charge by $(\pi\varepsilon_0\varepsilon_r\sigma k_BT)^{1/2}$, spring constant by k_BT/σ^2, and time by σ^2/D_0, where D_0 is the tracer diffusivity in the pure solvent. We have tested both Euler's method and the predictor-corrector integrator, and the comparison finds that the former with time step $\Delta t=0.0001$ can produce results with acceptable accuracy except for sufficiently low porosity. For particles with density of 1000 kg/m^3 and $\sigma \geqslant 5$ nm in aqueous solution, this time step is at least five times larger than the relaxation time of the particle momentum.

For each independent run, the tracer particle is initially placed at the center of the simulation box and a cubic lattice network (N^3) is generated as the initial configuration. The system is then equilibrated for 10^6 time steps ($\Delta t=0.0001$) followed by the generation of equilibrium configurations for the next 10^7 time steps to calculate the dimensionless mean-square displacement $\langle R(t)^2\rangle$ of the tracer

$$\langle R(t_m)^2\rangle = \frac{1}{M-m}\sum_{n=1}^{M-m} |\mathbf{r}_0(t_n+t_m)-\mathbf{r}_0(t_n)|^2, \tag{7}$$

where $t_n=n\Delta t$ and M denotes the number of total time steps. For particles with diameter of 5 nm in water at 25 °C, the dimensional Δt is 29 ps and the production period is 290 μs, in comparison with $\Delta t=1$ fs and the production time (10^6 time steps) of 1 ns in previous molecular dynamics simulations [14]. The tracer diffusivity normalized by D_0 is determined by

$$D = \frac{1}{6}\frac{d}{dt}\langle R(t)^2\rangle \tag{8}$$

as a function of time. The short-time diffusivity is identified by the D value in the limit of vanishing time, which nonetheless is still much longer than the momentum damping time to ensure the validity of Eq. (1). Determination of the long-time diffusivity, which is the asymptotic D for large enough time, could be computation intensive for certain cases. This is because for each case, a sufficient number (at least 20) of independent runs must be carried out, over which the long-time diffusivity is then averaged in order to attain a sufficiently accurate value. Otherwise, the fluctuating results would not show clear trends. On a Dell Precision 690 workstation, one run takes about 3–40 h, depending on the porosity and whether the system is charged. In addition to the tracer diffusivity, we also compute the radial distribution function for tracer-bead pairs and for bead-bead pairs in order to investigate the network microstructure experienced by the tracer.

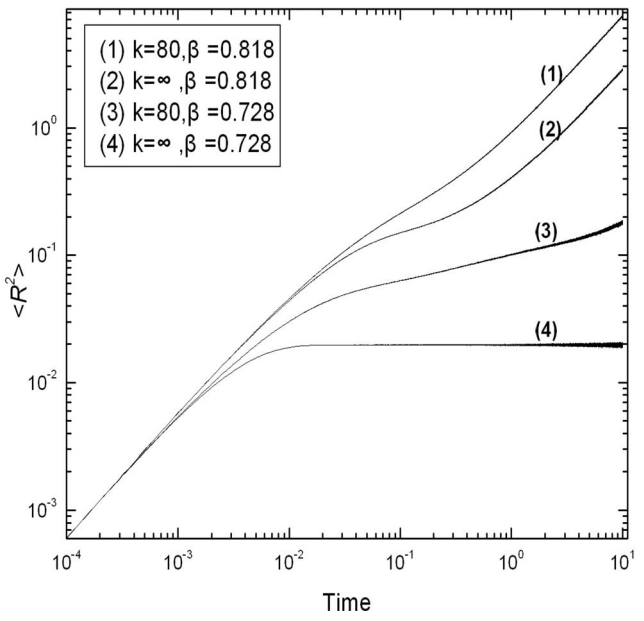

FIG. 2. Mean square displacement of the tracer in a 100% cross-linked uncharged network.

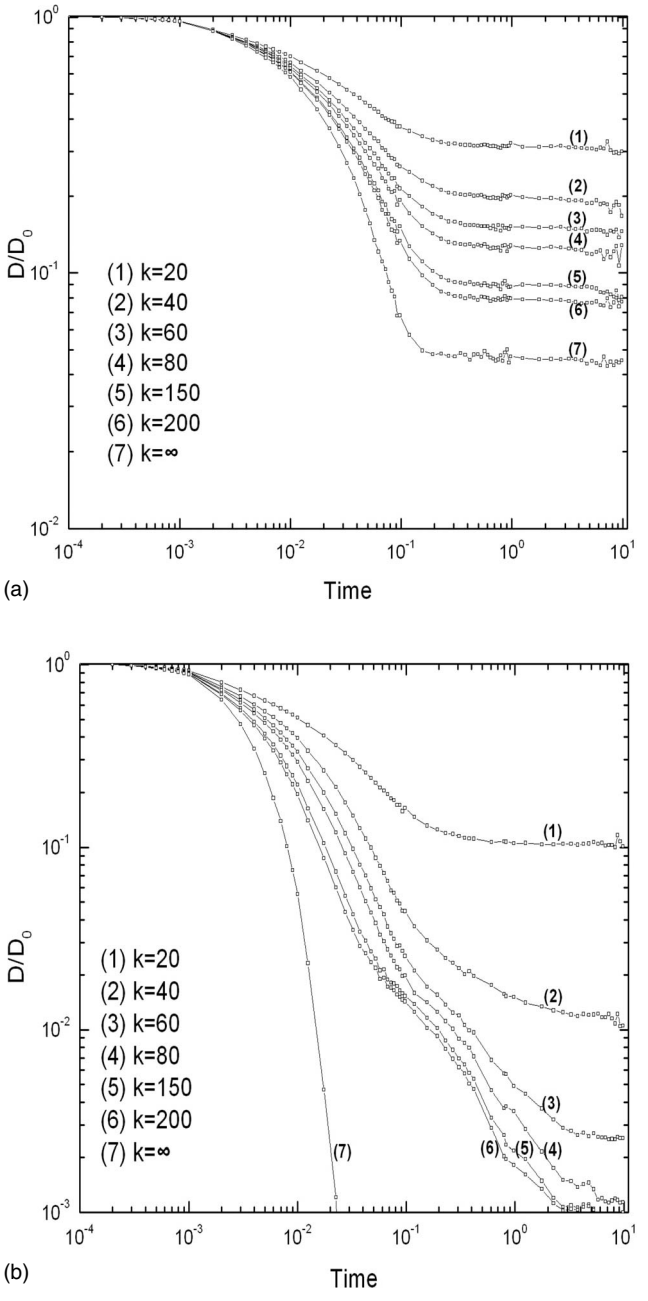

FIG. 3. Normalized tracer diffusivity versus time for a 100% cross-linked uncharged network with varying spring constant at $\beta=0.818$ (a) and 0.728 (b).

TABLE II. Normalized long-time tracer diffusivity for uncharged systems with 100% cross linking.

	D/D_0			
β	0.818	0.886	0.966	0.9995
$k=80$	0.116 ± 0.007	0.50 ± 0.04	0.88 ± 0.06	0.97 ± 0.06
$k=\infty$	0.048 ± 0.004	0.46 ± 0.04	0.85 ± 0.06	0.98 ± 0.08

III. RESULTS AND DISCUSSIONS

The system size effect has been examined by increasing N to ensure that the diffusivity results converge acceptably. For the investigated ranges of porosity in different cases, the appropriate system sizes used are summarized as follows. For the uncharged systems with 100% cross linking, we use $N=4$ except for $\beta=0.818$ and 0.728 ($N=10$). If the cross linking is less than 100%, $N=8$ is used except for $\beta=0.9995$ and 0.996 ($N=4$). For the charged systems, we use $N=4$ for 100% cross linking, and $N=8$ for the remaining cases. We also note that when l_0/σ (or β) is large enough, the excluded volume interactions between network beads can be neglected without incurring a significant error. For the cases of 100% cross linking, the error for tracer diffusivity is below 5% when $\beta>0.996$, but increases to 45–50% when $\beta<0.886$. The error is larger for the cases with a lower degree of cross linking.

A. Uncharged network

For an uncharged network, we investigate the effects of its porosity, flexibility, and cross-linking extent. In the present model, the flexibility of a 100% cross-linking gel can be adjusted by varying the spring constant. For a rigid network, a simple geometry analysis can be conducted to find that (1) the lowest network porosity to accommodate a tracer is $\beta=0.66$, and (2) when $\beta<0.815$, the tracer will be trapped permanently in the unit cubic cell where it is initially located. To illustrate this behavior, we plot the mean-square displacement $\langle R(t)^2\rangle$ against time in Fig. 2. One can find that $\langle R(t)^2\rangle$ becomes constant at long times for $k=\infty$ and $\beta=0.728$, indicative of the cage effect, whereas the transition from short-time to long-time diffusion can be clearly seen for $\beta=0.818$ (slightly higher than 0.815). Note that for our simulation of a rigid network, the network beads are fixed in space, rather than dynamical. Figure 3(a) plots the tracer diffusivity as a function of time for $\beta=0.818$. The asymptotic long-time diffusivity, which can be obtained when $t\geqslant 0.2$, shows a decreasing function of the spring constant. At this porosity, the excluded volume effect is strong, leading to substantial hindrance to the tracer diffusion. When the spring constant increases progressively, the network flexibility is

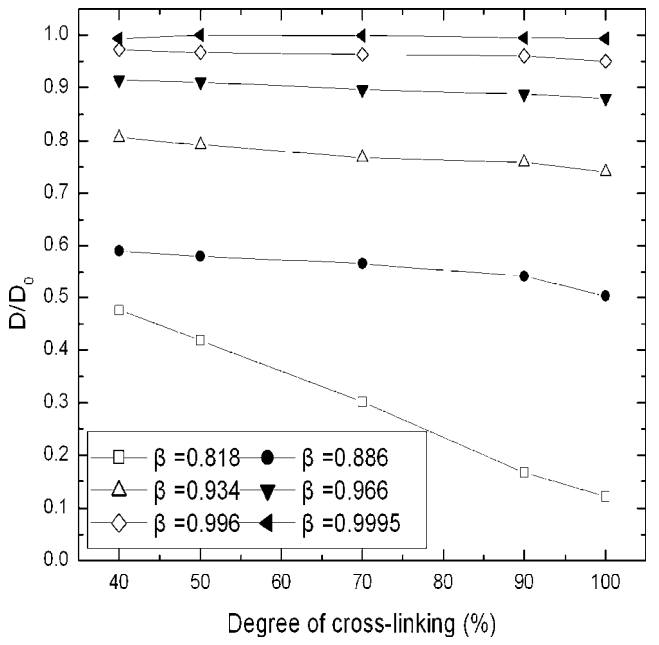

FIG. 4. Normalized long-time tracer diffusivity versus degree of cross linking for an uncharged network with $k=80$ and varying porosity.

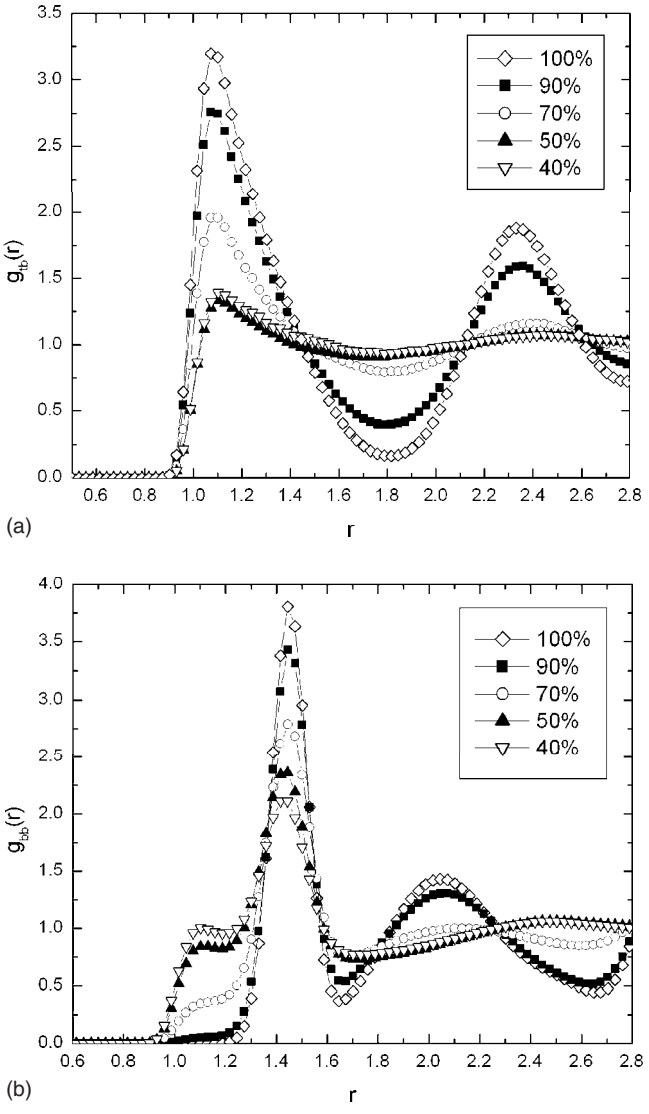

FIG. 5. Pair radial distribution function for an uncharged network with $k=80$, $\beta=0.818$, and varying degree of cross linking: (a) tracer-bead, (b) bead-bead.

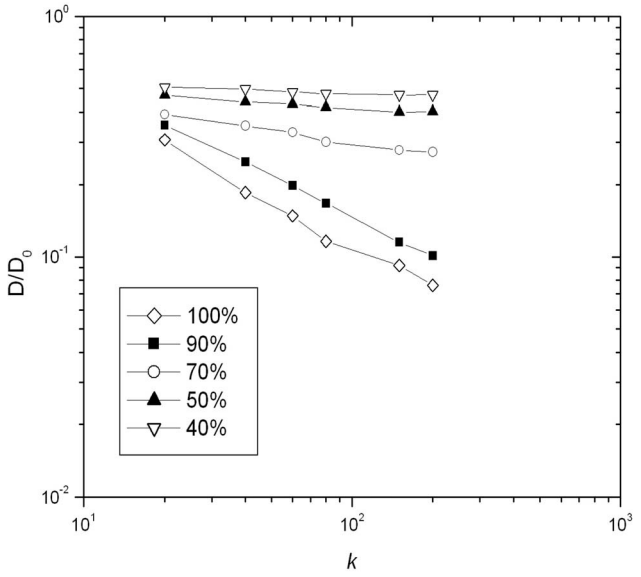

FIG. 6. Normalized long-time tracer diffusivity versus spring constant for an uncharged network with $\beta=0.818$ and varying degree of cross linking.

reduced, so is the positional fluctuation of the network beads. This reduction makes it more difficult for the tracer to diffuse away from a unit cubic cell to enter an adjacent one owing to the lower possibility for the formation of a larger opening as a pathway. Therefore, the long-time diffusion is slowed down.

When the porosity becomes lower ($\beta<0.815$), the tracer may get trapped in a unit cubic cell for a long time, depending on the network flexibility. The long-time diffusion is primarily controlled by the tracer escape mechanism. For a flexible network, such escaping could be possible, provided that the positional fluctuation of the network beads is strong enough (i.e., small enough k) to create sufficiently large openings for the tracer to pass through. This behavior can be seen in Fig. 3(b) for $\beta=0.728$. The long-time diffusivity can be reliably obtained for $k\leqslant 60$ within the time period investigated. For higher but finite k, in contrast, the diffusivity seems to level off only slightly at long times. In the limiting case of a rigid network, the long-time diffusion becomes anomalous with the diffusivity behaving as $t^{-3.2}$. The scaling, which reflects the rate of the diffusivity decaying to zero, is obtained from a linear fit to the curve in Fig. 3(b). Recently, Teixeira *et al.* applied dynamic light scattering to measure the diffusivity for latex particles (198 nm) in poly(methyl methacrylate) gel, and magnetic particles (60 nm) in polyacrylamide gel [19]. The particles, which are much larger than the gel mesh size, were added to the solution during the gel synthesis, resulting in the permanent entrapment within the gel. According to the simulation work of Licinio and Teixeira [17], the segment diffusion of a 3D flexible network is anomalous, and hence the long-time diffusivity of trapped particles should scale as $t^{-1.5}$ to follow the gel dynamics. Although permanent entrapment of tracer particles takes place in our rigid network at $\beta=0.728$, the network itself does not show any dynamics at all. This difference accounts for the faster decaying of the tracer anomalous diffusion obtained in the rigid network. For flexible networks, it can be seen from Fig. 3(b) that, when the spring constant increases, the tracer diffusivity at long times decreases more rapidly with time. However, the data analysis becomes difficult for large k due to the increased fluctuation of the simulation results, which is attributable to the strong spring force. Therefore, it is inconclusive as to whether the tracer diffusion remains Fickian or becomes anomalous for k between 80 and 200.

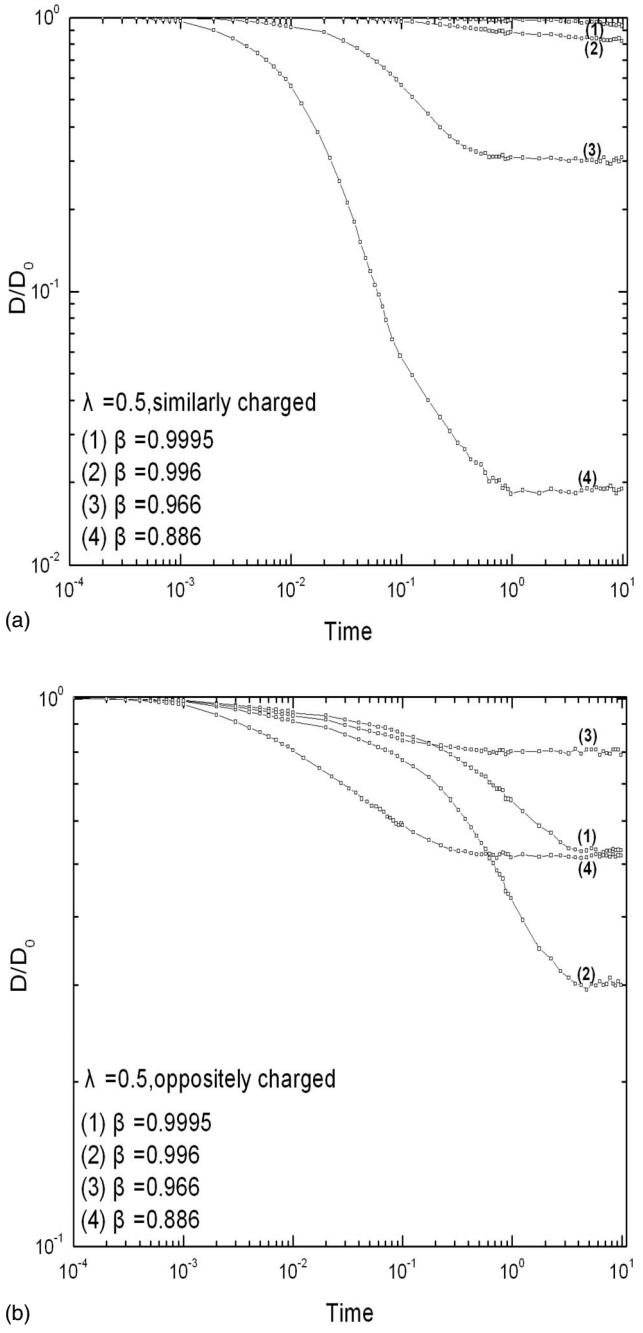

FIG. 7. Normalized tracer diffusivity versus time for a 100% cross-linked charged network with $k=80$, $\lambda=0.5$, $|Q|=12$, and varying porosity: (a) similarly charged; (b) oppositely charged.

Table II lists the long-time diffusivity for a rigid network and a flexible one of $k=80$ with varying porosity

TABLE III. Normalized long-time tracer diffusivity for similarly charged systems with $\lambda=0.5$ and 100% cross linking.

		D/D_0			
β		0.886	0.966	0.996	0.9995
$\|Q\|=12$	$k=80$	0.019 ± 0.002	0.31 ± 0.02	0.82 ± 0.07	0.93 ± 0.06
	$k=\infty$	0.0012 ± 0.0001	0.23 ± 0.02	0.85 ± 0.07	0.95 ± 0.07
$\|Q\|=18$	$k=80$	0.017 ± 0.001	0.07 ± 0.01	0.72 ± 0.06	0.93 ± 0.06
	$k=\infty$	$5.6\times10^{-4}\pm0.4\times10^{-4}$	0.03 ± 0.01	0.74 ± 0.06	0.95 ± 0.07

($\beta>0.815$). The largest difference in diffusivity between the two cases occurs at $\beta=0.818$, where the excluded volume effect is significant, but the permanent entrapment in the rigid network has not yet occurred. No comparison is made for $\beta<0.815$ because the tracer diffusion becomes anomalous in a rigid network.

The variation of long-time tracer diffusivity with the degree of cross-linking for $k=80$ and various porosities is shown in Fig. 4. Although the diffusivity is found to decrease generally with increasing cross linking, the variation becomes pronounced only for the network with low enough porosity, say $\beta=0.818$. A change in the degree of cross linking can lead to a change in the network structure. To explore this effect, we plot in Fig. 5(a) the radial distribution function of tracer-bead pairs $g_{tb}(r)$ for $k=80$ and $\beta=0.818$. The corresponding radial distribution function of bead-bead pairs $g_{bb}(r)$ is presented in Fig. 5(b). It can be seen from Fig. 5(b) that g_{bb} becomes more diffuse when the cross-linking extent is reduced, indicative of the formation of a weaker network structure. For such a structure, less obstructive paths can emerge to facilitate the tracer diffusion, as reflected by the lower probability of close tracer-bead encounters shown in Fig. 5(a).

To examine the effect of the spring constant, we plot the long-time diffusivity against the spring constant for $\beta=0.818$ and different cross-linking density on a logarithmic scale in Fig. 6. There appears to be a power-law behavior for 100% cross linking ($D/D_0\sim k^{-0.59}$). When the cross-linking density is decreased, the dependence of the tracer diffusivity on the spring constant becomes weaker, in particular for a degree of cross linking lower than 50%. The weaker dependence on the spring constant arises from the increased ease for the tracer diffusion due to the presence of less obstructive paths upon the removal of sufficient springs.

B. Charged network

For a charged network, we would like to address the physical parameters before presenting the simulation results. Taking a typical monomer size of about 0.3 nm, we consider the case where a network bead represents 30 monomers, each of which can carry an elementary charge. Based on a coiled state in good solvent, the bead diameter is about 5 nm and its dimensionless charge is about 12 if the degree of dissociation is 50%. The Debye screening length can vary from 1 to 10 nm when the ionic strength is decreased from $0.1M$ to $0.001M$. Therefore, it is reasonable to use a dimensionless charge of $O(10)$ for particles and a dimensionless Debye length of $O(1)$. Note that the size and charge of the tracer particle are comparable to those used by Miyata *et al.* [16]

We first consider the cases of 100% cross linking. Figures 7(a) (similarly charged) and 7(b) (oppositely charged) plot the tracer diffusivity against time for $\lambda=0.5$, $k=80$, and various network porosities when the dimensionless charge of each particle is $|Q|=12$. For the similarly charged cases, it can be seen that the long-time diffusion can be reached at $t\approx1$, which is longer than that for the uncharged counterpart [cf. Fig 3(a)], indicative of slower diffusion due to the charge effect. Analogous to the behavior in the uncharged system, the long-time diffusivity decreases with decreasing porosity. Table III shows the long-time diffusivity for $k=80$ and ∞; $|Q|=12$ and 18. A comparison with Table II finds that the tracer diffusivity is considerably smaller than that for its uncharged counterpart, when the porosity is low. For instance, the long-time diffusivities for $|Q|=12$ and $k=80$ are 0.31 and 0.019 for $\beta=0.966$ and 0.886, respectively, as compared to 0.88 and 0.50 for the uncharged counterparts. The decrease in diffusivity can be attributed primarily to the electrostatic interaction between the particles, leading to an additional repulsion experienced by the tracer when moving towards

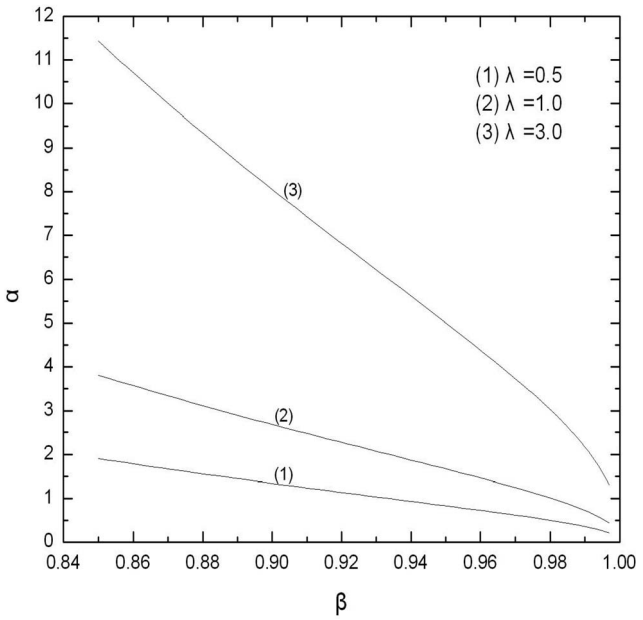

FIG. 8. Parameter for double layer overlapping as a function of network porosity.

TABLE IV. Normalized long-time tracer diffusivity for oppositely charged systems with $\lambda=0.5$ and 100% cross linking.

		D/D_0			
β		0.886	0.966	0.996	0.9995
$\lvert Q\rvert=12$	$k=80$	0.52 ± 0.02	0.79 ± 0.04	0.30 ± 0.04	0.53 ± 0.08
	$k=\infty$	0.52 ± 0.03	0.77 ± 0.06	0.28 ± 0.04	0.52 ± 0.07
$\lvert Q\rvert=18$	$k=80$	0.49 ± 0.04	0.56 ± 0.04	0.022 ± 0.004	0.04 ± 0.02
	$k=\infty$	0.55 ± 0.04	0.51 ± 0.03	0.005 ± 0.002	0.02 ± 0.01

network beads. Since λ is $O(1)$, this extra repulsion has a longer range than the steric effect. It is interesting to address the subtle effect of the network flexibility on the tracer diffusion. At a high porosity, the tracer will most likely encounter only one network bead at a time, thereby hardly experiencing the effects from other beads that are far away. The flexibility renders the network to behave like a cushion, allowing the encountered bead to retreat and the tracer to advance more. As a result, their encounter time on average is

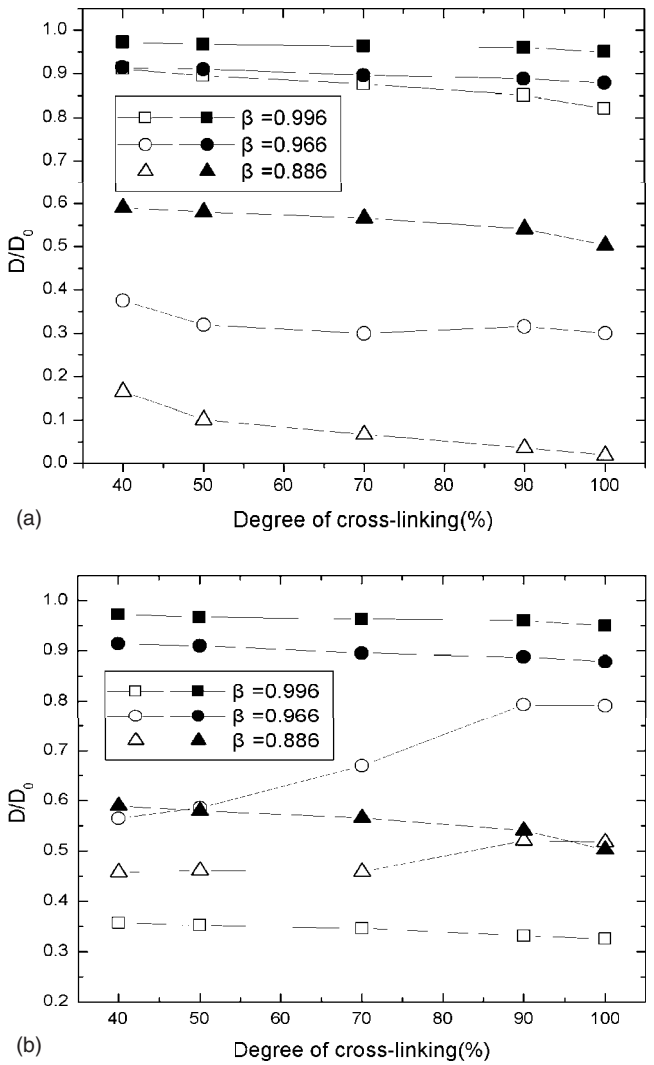

FIG. 9. Normalized long-time tracer diffusivity versus degree of cross linking for a charged network (hollow symbols) with $|Q|=12$, $\lambda=0.5$, and $k=80$: (a) similarly charged; (b) oppositely charged. The results for the corresponding uncharged counterparts are also shown (filled symbols) for comparison.

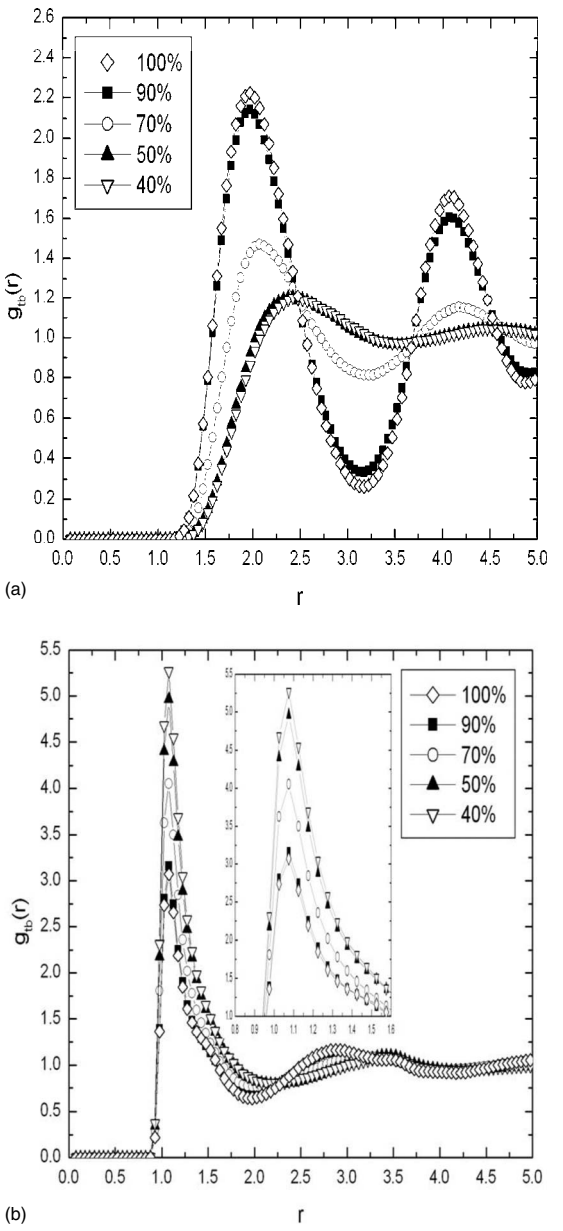

FIG. 10. Radial distribution function of bead-tracer pairs for a charged network with $k=80$, $|Q|=12$, $\lambda=0.5$, and $\beta=0.966$: (a) similarly charged (b) oppositely charged.

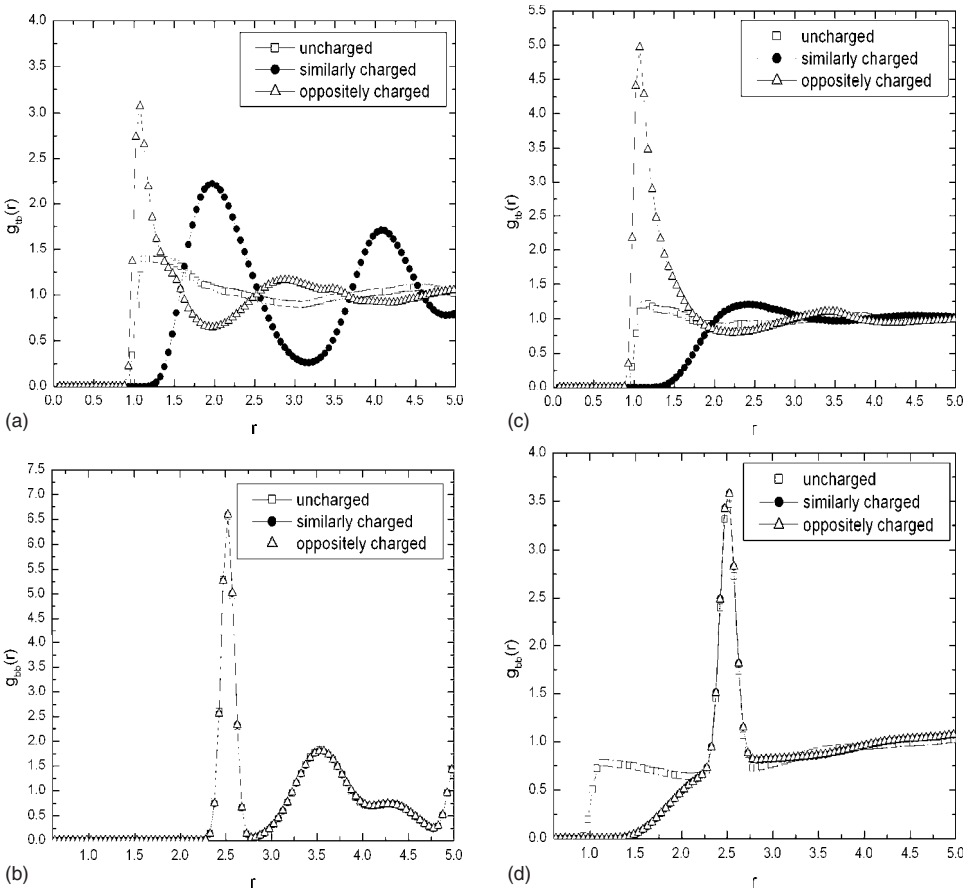

FIG. 11. Pair radial distribution function for a network with $k=80$, $|Q|=0$ or 12, $\lambda=0.5$, $\beta=0.966$: (a) tracer-bead (100% cross-linking); (b) bead-bead (100% cross linking); (c) tracer-bead (50% cross linking); (d) bead-bead (50% cross-linking).

increased, accounting for the slight decrease in the long-time diffusivity as compared to that in a rigid network. When the porosity is decreased to become low enough, the tracer may feel the effects from more than one network bead at a time, and the mechanism of tracer escaping becomes increasingly important. In addition, the collective repulsive electrostatic interaction causes the tracer to preferably take a path following an energy valley between network beads. For a flexible network, the positional fluctuation of the beads as well as the electrostatic repulsion exerted by the approaching tracer increases the possibility of the formation of a larger opening for the tracer to diffuse into another unit cell, thereby leading to a greater diffusivity than in the corresponding rigid network (see Table III).

For the oppositely charged cases, one can find from Fig. 7(b) that the tracer diffusivity is no longer a monotonic increasing function of the network porosity. For the two higher porosities ($\beta=0.9995$ and 0.996), the tracer diffusivity is much smaller than that for its similarly charged counterpart [cf. Fig. 7(a)]. This intriguing behavior can be explained by the electrostatic attraction between the tracer and nearby network beads. At high enough porosities, the tracer can interact with one network bead at a time, as mentioned earlier. When the tracer diffuses towards a bead by chance, the electrostatic attraction can cause the tracer to associate with the bead and stay around for some time until the fluctuating thermal energy becomes large enough for their breakup. Therefore, each of the network beads can be regarded as a temporary trap, impeding the tracer diffusion. Miyata *et al.* used a similar mechanism to explain the substantial decrease of tracer diffusivity in their simulation for a rigid network [16]. In the high-porosity regime, the diffusivity decreases with deceasing porosity, owing to an increase in the trap number density. However, a different behavior is observed when the network porosity is further reduced. At $\beta=0.966$, the diffusivity at long time becomes larger than those for the two prior cases. This interesting behavior is associated with the double layer overlapping between the network beads. The extent of double layer overlapping can be estimated by the parameter $\alpha=2\lambda/(l_0-\sigma)$, which becomes $O(1)$ for the onset of overlapping. Figure 8 plots α against β for three values of λ. For $\lambda=0.5$, α is 0.67 and 1.5 at $\beta=0.966$ and 0.886, respectively, as opposed to 0.11 and 0.25 at $\beta=0.9995$ and 0.996. The double layer overlapping leads to a decreased variation of the electrostatic interaction energy with position, namely, the tracer will experience a smaller electrical force when moving in the network. Therefore, the aforementioned effect of the temporary electrostatic traps is substantially weakened. Note that the tracer diffusivity remains lower than its uncharged counterpart at $\beta=0.966$, but becomes comparable at $\beta=0.886$. Table IV presents a comparison of the tracer long-time diffusivity between the flexible network ($k=80$) and the corresponding rigid network ($k=\infty$). It is interesting to find that while the tracer diffusivity for $|Q|=12$ differs only slightly between $k=80$ and ∞ for the four porosities, the difference becomes pronounced at $\beta=0.9995$ and 0.996 when $|Q|=18$. The larger tracer diffusivity in the flexible network may be attributed to an increased ease of the tracer escaping

from an entrapping bead, because both can undergo thermal motion.

The effect of cross-linking extent on the tracer diffusivity is examined for $\lambda=0.5$, $|Q|=12$, and $k=80$, with the results shown in Fig. 9. The results for the corresponding uncharged cases are also presented for comparison. For similarly charged cases [Fig. 9(a)], the diffusivity decreases weakly with increasing cross-linking, analogous to the uncharged system. The opposite behavior, however, could be found for the oppositely charged counterpart at $\beta=0.886$ and 0.966 [see Fig. 9(b)].

To explore how the entrapment effect changes with varying cross-linking extent, we plot g_{tb} for the oppositely charged case with $\beta=0.966$ in Fig. 10(b), while the result for its similarly charged counterpart is shown in Fig. 10(a) for comparison. Differences can be clearly seen from the two figures. For the oppositely charged case, the first peak is sharper and stronger, occurring always at a lower $r(\approx 1)$, but the waviness of g_{tb} subsides faster as r is increased. This behavior is even more pronounced at lower β. For instance, the first peak value can be as high as 33 for $\beta=0.996$ and 40% cross linking, although the figure is not presented. It evidently indicates the frequent occurrence of tracer entrapment via the electrostatic attraction. Also, it is noteworthy from Fig. 10(a) that, for the oppositely charged cases, the first peak value decreases with increasing cross linking, indicative of the weakened entrapment effect. This interesting behavior can be explained again by the overlapping of double layers, leading to the decreased electrostatic force when the porosity is low enough and the degree of cross linking is high. In a network with weaker structure (a lower degree of cross linking), however, some of the network beads may not have as many nearby neighbors to interfere, and can thus trap the tracer more strongly, reflected by the stronger peak in Fig. 10(b) and the lower diffusivity in Fig. 9(b). For the similarly charged cases, in contrast, the first peak shifts to a larger r and becomes weaker with decreasing cross linking [see Fig. 10(a)]. In addition, the first peak is also located at greater r when the porosity is increased, although no graphical results are shown here.

It is interesting to compare the radial distribution function between charged and uncharged system. In Figs. 11(a) and 11(b), we plot g_{tb} and g_{bb} for the 100% cross-linking network with $\lambda=0.5$, $|Q|=12$ or 0, and $k=80$. Similar plots are made for 50% cross linking in Figs. 11(c) and 11(d). One can clearly see from Fig. 11(b) that g_{bb} curves coincide for the three cases, indicating the same static structure of 100% cross-linking network. In contrast, g_{tb} presented in Fig. 11(a) exhibits a significant difference among the three cases. For the oppositely charged case, the electrostatic attraction leads to the strong first peak located at $r\approx 1$, representing the near contact between the tracer and a bead. For the similarly charged case, the first peak becomes weaker and shifts considerably to $r\approx 2$, because the electrostatic repulsion prevents the tracer from getting very close to a bead. For the uncharged system, in contrast, no obvious characteristic separation distance is seen. When the cross-linking degree is decreased to 50%, the charge effect causes g_{bb} to differ from that of the uncharged case for $r<2.2$, as seen in Fig. 11(d). This difference can be explained by the weaker network structure that allows a closer approach between the uncharged beads. We find from Fig. 11(c) that g_{tb} becomes more diffuse for the similarly charged case.

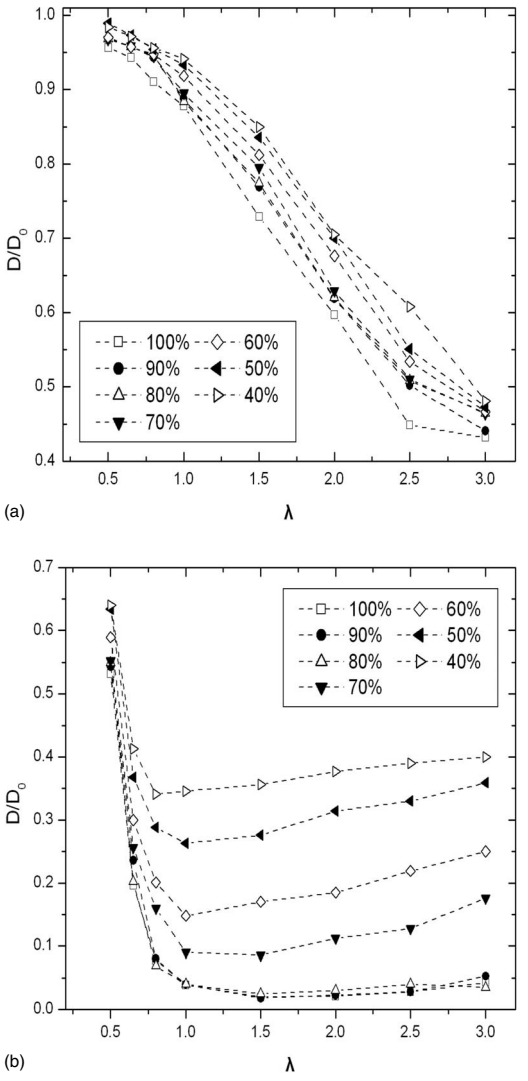

FIG. 12. Normalized long-time tracer diffusivity versus dimensionless double layer thickness for a charged network with $k=80$, $|Q|=12$, and $\beta=0.9995$: (a) similarly charged; (b) oppositely charged.

For the two different charge cases, the effect of double layer thickness on the tracer diffusivity is presented in Fig. 12 for $\beta=0.9995$, $|Q|=12$, and $k=80$. One can see that the diffusivity for the oppositely charged case is not a monotonic function of the double layer thickness, as opposed to the similarly charged counterpart. For the former, the slight increase in diffusivity with increasing λ is attributable to the stronger double layer overlapping, thereby leading to the weakened electrostatic entrapment effect and the change in microstructure. It should be noted that a further increase in double layer thickness would require a larger system size to maintain the accuracy and even to ensure the validity, because of the increased range of the electrostatic interaction. Our testing finds that, at sufficiently large λ and small β, the projection of constant energy surfaces can show cusps, and thus the calculated interaction force becomes nonphysical.

This problem can in principle be resolved by using a larger N, which will then prolong the simulation however.

IV. CONCLUSION

A coarse-grained Brownian dynamics simulation has been employed to study the behavior of tracer particles in a gel network under the free draining condition. The simple mesoscopic model based on a bead-spring cubic lattice allows us to explore the tracer diffusion qualitatively without a need to implement the structural details of a realistic gel. We focus on four factors: network porosity, flexibility, degree of cross linking, and electrostatic interactions. For low enough porosities, an increased flexibility or reduced cross linking can considerably increase the tracer diffusivity, owing to the high possibility for the formation of larger openings for the tracer to escape from a unit cell to an adjacent one. The electrostatic interaction gives rise to distinct behaviors between similarly and oppositely charged cases. The tracer diffusivity for the latter case is not a monotonic function of the network porosity and double layer thickness. This interesting behavior is ascribed to the tracer entrapment by the network beads due to the electrostatic attraction. The entrapment effect is strong at high porosities, because the tracer-bead pair can hardly be interfered by remaining beads, which are far away. At low enough porosity, the tracer diffusivity may also increase with increasing cross linking.

Finally, we would like to address the negligence of hydrodynamic interaction in the present study. In the first place, it might be justified by the likelihood of considerable hydrodynamic screening for our concentrated system. Hydrodynamic interaction is long ranged in nature, and can in principle be examined using available hydrodynamic models, such as the Rotne-Prager tensor, together with the Ewald-sum technique. However, the corresponding computation will become rather intensive. Since the primary objective of this study is to explore the effect of network properties to understand how the tracer diffusion is affected qualitatively, we avoid the complicated computation incorporating the hydrodynamic interaction. Such an approach may speculatively lead to overestimated diffusivities. It is surely interesting and worthwhile to investigate this overlooked interaction in future.

ACKNOWLEDGMENT

This work is financially supported by National University of Singapore through Grant No. R279-000-203-112.

[1] T. G. Mason and D. A. Weitz, Phys. Rev. Lett. **74**, 1250 (1995).
[2] A. S. Hoffman, A. Afrassiabi, and L. C. Dong, J. Controlled Release **4**, 213 (1986).
[3] S. K. Sahoo, T. K. De, P. K. Ghosh, and A. Maitra, J. Colloid Interface Sci. **206**, 361 (1998).
[4] T. G. Park, Biomaterials **20**, 517 (1999).
[5] K. Sawahata, M. Hara, H. Yasunaga, and Y. Osada, J. Controlled Release **14**, 253 (1990).
[6] R. Chang and A. Yethiraj, J. Chem. Phys. **118**, 6634 (2003).
[7] T. Zhou and S. B. Chen, J. Chem. Phys. **122**, 124905 (2005).
[8] T. Zhou and S. B. Chen, J. Chem. Phys. **124**, 034904 (2006).
[9] C. Stoltz, J. J. de Pablo, and M. D. Graham, J. Chem. Phys. **126**, 124906 (2007).
[10] S. Sunderrajan, C. K. Hall, and B. D. Freeman, J. Chem. Phys. **105**, 1621 (1996).
[11] T. R. Cuthbert, N. J. Wagner, M. E. Paulaitis, G. Murgia, and B. D'Aguanno, Macromolecules **32**, 5017 (1999).
[12] O. Durr, T. Volz, and W. Dieterich, J. Chem. Phys. **117**, 441 (2002).
[13] P. A. Netz and T. Dorfmuller, J. Phys. Chem. B **102**, 4875 (1998).
[14] C. Oldiges and T. Tonsing, Phys. Chem. Chem. Phys. **2**, 5630 (2000).
[15] P. A. Netz and T. Dorfmuller, J. Chem. Phys. **103**, 9074 (1995).
[16] T. Miyata, A. Endo, T. Ohmori, M. Nakaiwa, M. Kendo, K.-I. Kurumada, and M. Tanigaki, J. Chem. Eng. Jpn. **35**, 640 (2002).
[17] P. Licinio and A. V. Teixeira, Phys. Rev. E **56**, 631 (1997).
[18] A. V. Teixeira and P. Licinio, Europhys. Lett. **45**, 162 (1999).
[19] A. V. Teixeira, E. Geissler, and P. Licinio, J. Phys. Chem. B **111**, 340 (2007).
[20] R. Hogg, T. M. Healy, and D. W. Fuerstenau, Trans. Faraday Soc. **62**, 1638 (1966).
[21] G. R. Wiese and T. M. Healy, Trans. Faraday Soc. **66**, 490 (1970).